Journal of Power Sources 265 (2014) 262–272

Contents lists available at ScienceDirect

Journal of Power Sources

journal homepage: www.elsevier.com/locate/jpowsour

Experimental investigation on heat pipe cooling for Hybrid Electric Vehicle and Electric Vehicle lithium-ion battery

Thanh-Ha Tran [a,b,c,*], Souad Harmand [a,b], Bernard Sahut [c]

[a] Université Lille Nord de France, 59000 Lille, France
[b] UVHC, TEMPO, 59313 Valenciennes, France
[c] PSA Peugeot Citroen, France

HIGHLIGHTS

- A heat pipe cooling system was designed and a full size prototype was built.
- Experimental investigation was performed under 3 input power levels.
- Several cooling conditions were experimented to minimize the power consumption.
- The system's performance was evaluated under different grade road conditions.

ARTICLE INFO

Article history:
Received 20 September 2013
Received in revised form
16 April 2014
Accepted 25 April 2014
Available online 9 May 2014

Keywords:
Heat pipe
Transient input power
Cooling system
Lithium-ion battery
Hybrid electric and electric vehicle

ABSTRACT

In this work, we explored the use of heat pipe as cooling device for a specific HEV lithium-ion battery module. The evaporator blocks of heat pipe modules were fixed to a copper plate which played the role of the battery cooling wall. A flat heater was glued to the other surface of the copper plate and reproduced heat generated by the battery. The temperature at the cooper plate/heater interface corresponds to that of the battery module wall. An AMESim model of the battery was developed to estimate the cells' temperature within the battery. In inclined positions, a very slender evolution of the cooper plate/heater interface temperature was noticed, which means heat pipe works efficiently under different grade road conditions. Even though natural convection and chimney effect are not enough, coupling heat pipes with a confined ventilation structure is an efficient way to keep cells' temperature within its optimal range with an even temperature distribution. Furthermore, only low rate ventilation is necessary, which helps avoid parasitic power consumption and noise level in the vehicle.

1. Introduction

Lithium-ion batteries possess a high energy density compared with other secondary batteries; consequently, they are highly recommended as power sources for hybrid and electric vehicles (HEV/EV) to provide longer driving range and faster acceleration. However, lithium-ion batteries are extremely sensitive to low and high temperatures. As the temperature falls to below −10 °C, the performance of lithium-ion batteries deteriorates drastically [1,2]. At high temperature, lithium-ion batteries are extremely prone to thermal runaway [3]. For security reasons, a battery thermal management system (BTMS) always includes an internal switch which is opened if the battery is operated outside of its operating temperature range. This can prevent fire or explosion risks but the battery would be temporarily unavailable. Fuel economy of HEV and the driving range of EV are consequently affected. Furthermore, a number of works have elucidated that lithium-ion batteries calendar life [4,5] and cycle life [6–8] degrade quickly if kept or used at high temperature.

The goal of a cooling system is to keep the cells within its optimal temperature range, which offers the best balance between performance and ageing. The temperature distribution within the pack should be even because temperature gradient could lead to different ageing levels between cells and therefore, different charge/discharge behaviours for each cell [9,10]. For a Li-ion battery, the cells' temperature should not exceed 50 °C, the optimal temperature range is between 35 and 40 °C and the temperature gradient should be less than 5 °C [11,12]. In addition, the cooling system has to meet the requirements of the vehicle such as:

* Corresponding author. UVHC, TEMPO, 59313 Valenciennes, France.
E-mail address: thanh-ha.tran@hotmail.fr (T.-H. Tran).

http://dx.doi.org/10.1016/j.jpowsour.2014.04.130
0378-7753/

Nomenclature

A	cooling wall area [m^2]
Cp	specific heat capacity [kJ kg^{-1} K^{-1}]
dU_o/dT	entropy coefficient [V K^{-1}]
dt	time step [s]
h	overall heat transfer coefficient [W m^{-2} K^{-1}]
i	number of the surrounding nodes [−]
I	cell current intensity [A]
m	mass [kg]
q	heat exchanged [W]
R	thermal resistance [°C W^{-1}]
T	temperature [K]
U_o	open-circuit potential [V]
U	measured cell potential [V]
V	velocity [m s^{-1}]
P	heat produced by heater [W]

Indices

a,b	resin nodes
amb	ambient
air	air
cell	cell
condenser	fin block
equi	related to the heat pipes cooling system
evaporator	copper plate/heater interface
i	related to the surrounding nodes
max	maximal value
resin	resin matrix
wall	battery module wall

Greek symbols

λ	thermal conductivity [W m^{-1} K^{-1}]
Φ	heat generated by cell [W]

reliable, compact, lightweight, easily accessible for maintenance, low cost, and low power consumption.

Up to now, battery cooling systems may use air, liquid (water/oil/refrigerant), phase change materials (PCM), or a combination of these methods. Each solution has its advantages and weaknesses. Air cooling solution can be passive (i.e., only the ambient environment is used) or active (i.e., a built-in source provides heating and/or cooling) [13]. The obvious benefit of air-cooled systems is the elimination of on-board chiller unit and coolant pump; leading to savings in energy consumption and weight. However, air convection can't be sufficient for heat dissipation from battery under stressful and abuse conditions. Consequently, the non-uniform distribution of temperature within battery pack becomes inevitable [14,15]. Compared with air cooling, liquid cooling offers higher cooling capacity at similar parasitic pump/fan power [13] but is heavier, and costlier due to the use of pump, tank, heat exchanger … Maintenance and repair of liquid cooling systems are also complicated and costly. PCM systems have high thermal energy storage capacity thanks to the use of latent heat and therefore can maintain the battery temperature relatively constant and near to the melting point during operation [16–18]. However, the weak point that has limited widespread use of PCM system is its insufficient long term thermal stability.

It is well known that heat pipe has very high thermal conductivity and can maintain homogeneously the evaporator surface at nearly constant temperature. Moreover, this device has flexible geometry which can fit variable area spaces. These attractive characteristics make heat pipe a promising candidate for HEV/EV battery cooling. Up to now, the only concern that has limited the large use of heat pipe system is its high cost due to the complicated fabrication process and the use of copper, an expensive metal, as wick and wall material. However, recent researches on aluminium heat pipe manufacturing [19,20] have revealed efficient and reliable way to decrease the heat pipe cost. Furthermore, the use of aluminium also helps reduce the weight of the cooling system, which is highly appreciable in HEV/EV application.

Previously, Mahefkey et al. [21] and Zhang et al. [22] have judged heat pipe to be suitable to mitigate the temperature of Ni–Cd and the Ni–MH battery respectively. Concerning Li-ion battery, Wu et al. [23] have reported that the cell temperature could be significantly reduced using heat pipe with aluminium fin on the condenser section, especially with the help of a cooling fan at the condenser section. More recently, Rao et al. [24] have investigated experimentally the cooling performance of tube heat pipes with condenser sections cooled by a water module. The battery maximum temperature has been controlled below 50 °C when the heat generation rate was lower than 50 W. Coupled with the desired battery temperature gradient, the heat generation rate should not exceed 30 W. In other words, with well-designed heat pipes, the temperature rise and temperature difference of power batteries can be effectively controlled within desired range.

In this work, we explored the use of tube heat pipe as cooling device for a specific HEV lithium-ion battery module. The thermal behaviour of the heat pipe cooling system was evaluated under various inclined positions corresponding to different grade road conditions. Natural cooling and chimney cooling at condenser section were also experimented. In addition, to enhance heat evacuation at the heat pipe condenser, two different air forced convection configurations were considered and compared. Finally, we investigated the thermal performance of the heat pipe system under a wide range of evaporator input power, corresponding to heat generated by the battery under different HEV power demands.

2. Experimental set-up

2.1. The battery module description

The battery module was made of 14 cylindrical cells (6.5 Ah of capacity, 38 mm in diameter, 142 mm in height). Cells were implemented in a thermally conductive and electrically insulating resin matrix which helped keep cells in place and increase the mechanical rigidity of the module. Moreover, the matrix enhanced the heat transfer between the cells and the aluminium module walls, as well as the electric insulation between the cells.

During charge and discharge, heat generated by cells can be considered to be the sum of the resistive heat and the entropic heat [25–29]. Consequently, the global heat generated can be determined by:

$$\phi = (U_o - U) - IT\frac{dU_o}{dT} \quad (1)$$

In order to maintain the cells within their optimum temperature range, heat generated needed to be evacuated through the module walls. The two walls corresponding to the two ends of the cells could not be used for cooling purpose. Indeed, one of the two walls was intended for bus bars and electric module installation and the other was used for degassing system implement. Among the four

remaining walls of the battery module, optimal thermal performance could be achieved by applying cooling devices to the two larger ones (168 mm in height by 286 mm in large) as shown in Fig. 1.

The magnitude of the overall heat generation rate by battery module varied according to the power demand of the HEV. A series of experiment was performed with a battery prototype which is similar to the battery presented in Fig. 1, except that the prototype had heat sinks embedded in its two lateral walls. These tests have been performed under charge sustaining mode (the SOC over a driving profile may increase and decrease but will, on the average, remain at its initial level). The current profile under charge sustaining mode was illustrated in Fig. 2. Two current levels have been experimented: I = ±10C and I = ±12C. The duration of each current pulse was 80 and 70 s respectively. SOC fluctuation was slightly over 20% with a mean value of 50%. The 12C discharge current corresponded to a very high power demand from the vehicle. Air forced cooling ventilation was used in order to keep cells within its optimal operating temperature range (between 35 and 40 °C). The temperature, tension and current of the cells were measured during operations thanks to battery electronic module which was connected to the computer using CANalyzer software. Using these experimental data, we calculated the mean heat for every charge–discharge cycle of the charge sustaining profiles. The effect of the entropic heat generated during the charge haft cycle was considered cancelled by that during the discharge haft cycle. Indeed, under steady state, the cell temperature was constant. Consequently, the entropic heat generated during the charge haft cycle equalled to the opposite of the entropic heat generated during the discharge haft cycle. When the cell temperature was not constant, the temperature elevation within the charge/discharge haft cycle was small (less than 1 K). Under this condition, the entropic heat during the charge haft cycle could be considered to be cancelled by that of the discharge haft cycle. Fig. 3 presents the heat calculated for tests under 10C and 12C current levels. We can see that after stabilization, the heat generated was 8.5 W cell^{-1} for the lower current level and 11 W cell^{-1} for the higher one. Consequently, the heat generated by the battery module under 10C and 12C current levels was 120 W and 154 W respectively.

2.2. The heat pipe cooling system description

The heat pipe cooling system designed for the battery module aforementioned consisted of four cooling modules. Each cooling module included seven tube heat pipes. These tubes were made of copper and had an outer diameter of 7 mm. The capillary structure included 50 helical grooves and the working fluid was demineralized water. The condenser section of each tube was bent at an angle of 121°. Fig. 4a presents the schema of the tube heat pipe and Fig. 4b shows the details of its capillary structure.

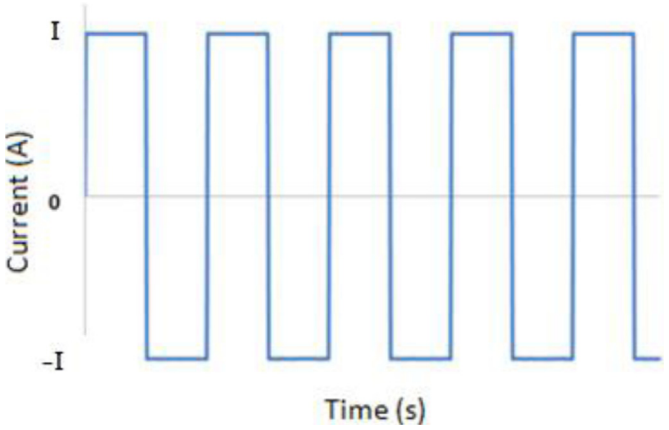

Fig. 2. Illustration of charge sustaining current profile.

To form the cooling module, the evaporator sections of these heat pipes were inserted in an aluminium block and aluminium fins were added to the condenser parts. The aluminium blocks of the four cooling modules were aimed to be fixed to the two battery cooling walls as illustrated in Fig. 5.

2.3. Experimental set-up

Due to the heat sinks embedded to the battery module wall, experimental investigation on the thermal performance of heat pipe could not be performed by attaching heat pipe directly to the

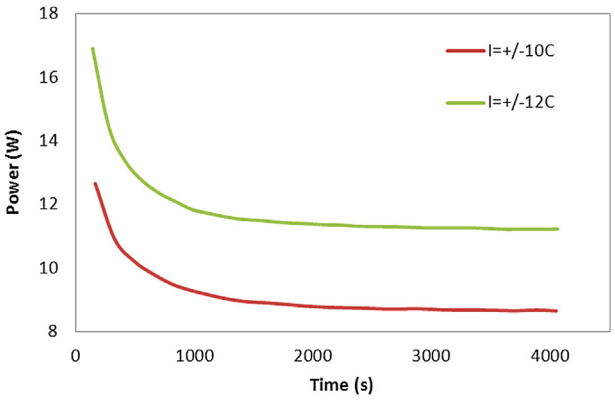

Fig. 3. Heat calculated for tests under 10C and 12C current levels.

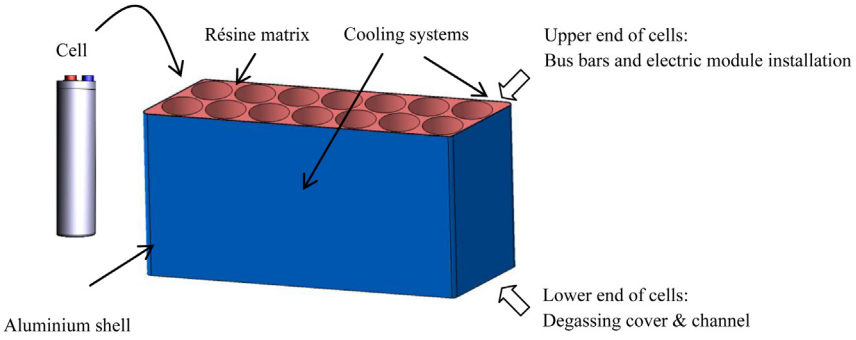

Fig. 1. Battery module.

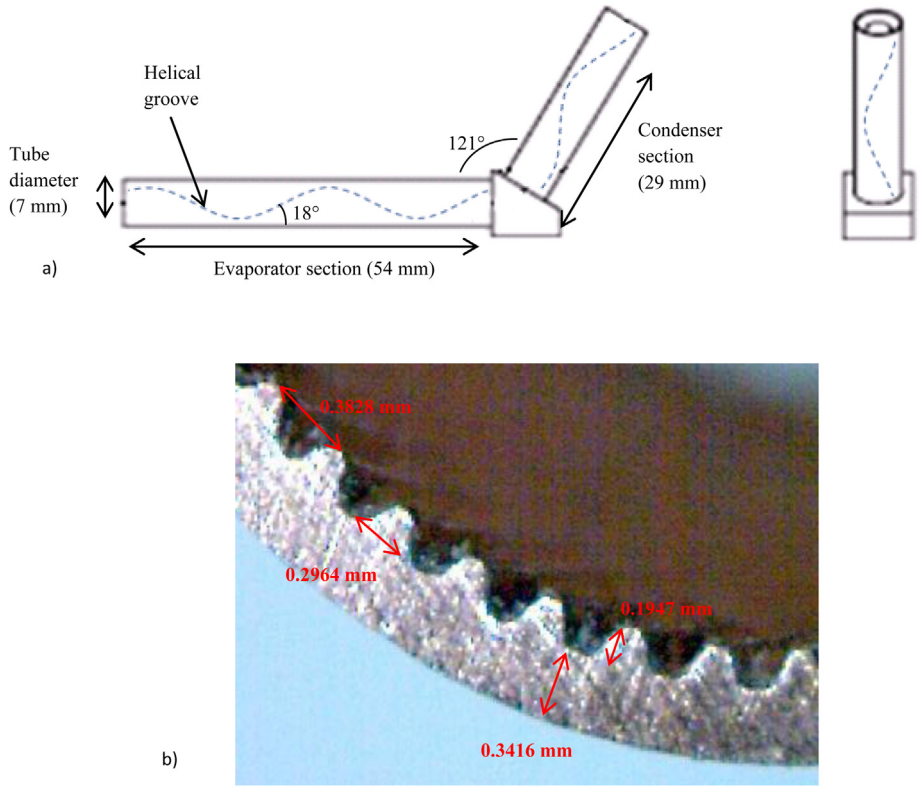

Fig. 4. Schematic of the tube heat pipe (a) and its capillary structure (b).

battery prototype. Instead, we worked with a thin cooper plate which played the role of one of the battery cooling walls and consequently, had identical dimensions to that of the cooling walls. Two cooling modules were fixed to one face the copper plate and a film heater was glued to the other face. Thermal grease was used to enhance the interfacial thermal conductance. To make sure that heat produced by the heater was dissipated in to the surround air only through the cooling modules, the back surface of the film heater was insulated.

A heater was plugged to a DC regulated power supply used to produce heat generated by cells. Assuming that the heat amount dissipated through the upper, lower and the two smaller lateral walls was negligible and taking into account the symmetry of the battery module, the heat arrived to each cooling wall at steady state is equal to 50% of the total heat produced by cells in the module. Heat pipe cooling modules were experimented under 3 power levels: 38 W, 54 W and 84 W, which corresponded to the battery global heat generation rates of 76 W, 108 W and 168 W respectively.

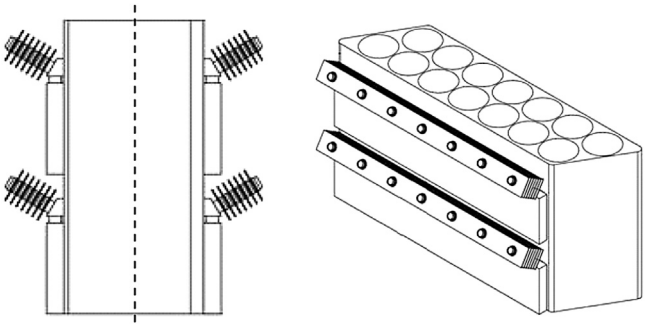

Fig. 5. The battery-cooling system assemblage.

We can see in Table 1 that the two higher experimented power levels correspond to the magnitude of the heat generated by the battery module under 10C and 12C current levels.

Temperature at different locations of the experiment apparatus was measured for each system using six K-type thermocouples with uncertainty of ±1.5 °C (Fig. 6). The accuracy of the thermocouples was checked using an infrared thermal camera with a spectral range of 7.5–13 μm, a resolution of 0.01 °C and an accuracy of ±2 °C. For this purpose, four black spots were painted on the aluminium block and the fin block of each heat pipe cooling module. The heater was turned on during few moments then shut off. During this operation, temperatures indicated by the thermocouples on the two condenser blocks corresponded to those measured at the black spots of the condenser blocks. The temperatures indicated by the thermocouples on the copper plate/heater interface were slightly higher than those given by the infrared camera for the two the aluminium blocks. This meant the temperature measured with thermocouples was highly accurate. The slim deviation ($\Delta T < 2$ °C) between the temperatures on the

Table 1
Heat generated by the battery modules and used for experimental investigation of the heat pipe cooling modules.

	Heat generated by the battery prototype		Heat used for experimental investigation of the heat pipe cooling modules	
HEV power demands	Current rates	Heat generated by the module	Heat produced by heater	Battery global heat generation rates
Moderate			38 W	76 W
High	10C	119 W	54 W	108 W
Very high	12C	154 W	84 W	168 W

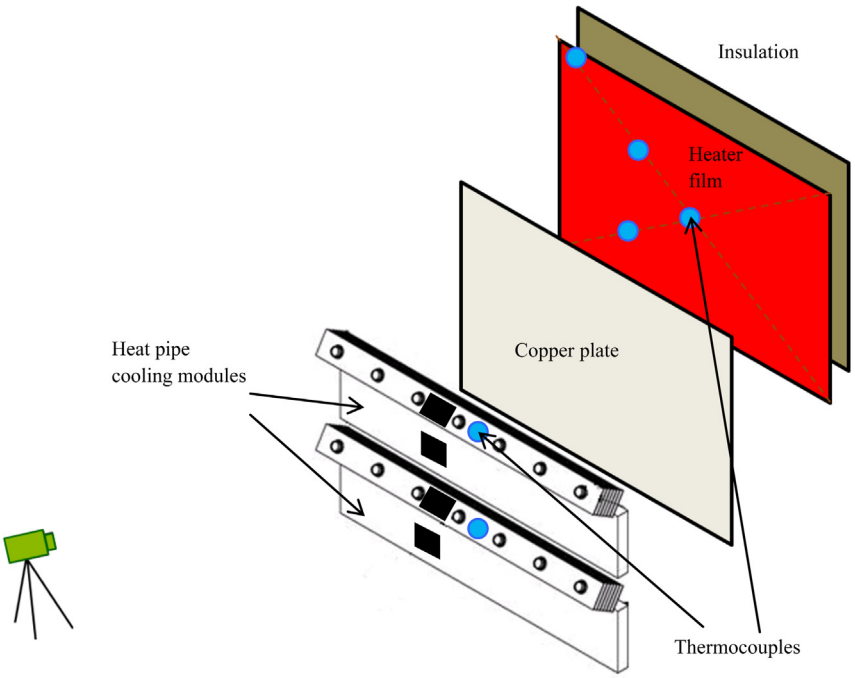

Fig. 6. Schematic of the experimental set-up.

aluminium blocks and those at the copper plate/heater interface could be explained by the effect of natural convection at the aluminium block surfaces.

In our application, the cooling modules were aimed to be used in vertical position. However, the evaluation of the cooling performance under uphill and downhill drive conditions was necessary for a vehicle application. Common roads were usually graded below 10% (5.71°). Inclines of over 20% (11.31°) were rare and maximum known incline on public streets were 37% (20.31°). Hence, heat pipe in vertical positions was respectively inclined with an angle of 20° and −20° in order to evaluate the impact of inclination to the thermal performance of the system (Fig. 7). Experiments in horizontal position were also performed.

In order to enhance heat dissipation at the condenser section, some air ventilation solutions were experimented. To reduce the power consumption, we first thought of a chimney effect. The copper plate-cooling modules assemblage was confined and a chimney was added to the top of the confined system. It is well known that the air velocity is in proportion with the height of the chimney. However, because of the constraint on the space allocated for the battery in the vehicle, the height of the chimney was limited.

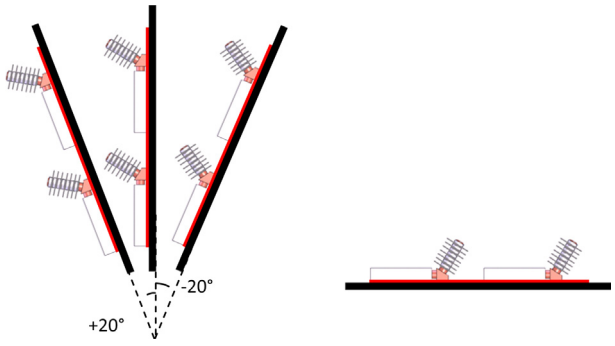

Fig. 7. Heat pipe cooling systems in various positions.

A schema of the chimney installation is shown in Fig. 8a. For higher heat dissipation capacity, air could be blown through the fins of the condenser using fans. Two configurations were used. In the first one, two flow channels using in total six helicoidal fans (80 × 80 mm of dimension) were installed to blow air in parallel toward the two condenser sections (Fig. 8b). In the second configuration, the copper plate-cooling modules assemblage was confined like in the case of chimney effect. Air was blown from the bottom of the confined system using a row of three helicoidal fans. The condenser blocks were cooled in series (Fig. 8c).

The fan could be driven between about 15% and 95% of the rated fan speed using pulse-width-modulation (PWM) control. For each fan speed level, the air velocity was measured for both the configurations using a hot-wire anemometer with measuring range from 0.15 to 30 m s^{-1}. At 15% PWM, the velocity of the air exiting the upper condenser block of the first and the second configuration was 1.2 m s^{-1} and 1.5 m s^{-1} respectively. In order to evaluate the thermal performance of heat pipe cooling at even lower air velocity, the fan inlet area could be obstructed. Table 2 illustrates the aspiration surface of the fan row and how fans were obstructed.

Each test condition was experimented three times and the reproducibility was found to be good. For all of the tests, the temperatures measured at different locations of the cooper plate/heater interface were very close to each other and the margin was less than 1 °C. Hence, only the mean temperature is reported in this paper.

3. Results and discussion

3.1. AMESim model of the battery module

In a configuration such as shown in Figs. 1 and 6, cooling devices were not in direct contact with cells but the battery module walls. Consequently, temperature measured at the heater/cooling system interface in our experiment corresponded to the temperature at the resin matrix/aluminium shell interface of the battery module and there was a temperature gradient between the resin matrix/

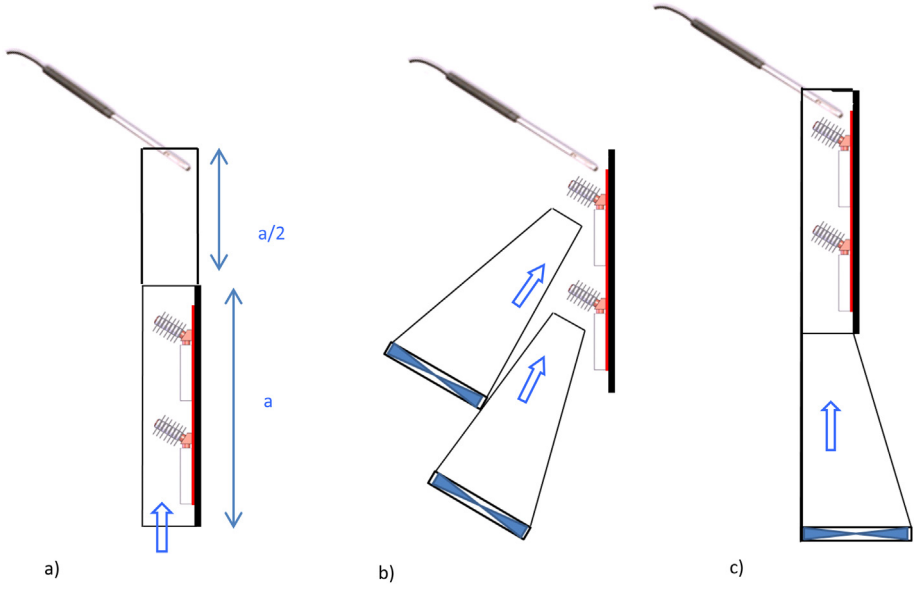

Fig. 8. Air chimney installation (a) and air forced cooling configurations (b, c).

aluminium shell interface and cells. In order to estimate cell temperature at different locations of the module, we use numerical simulation in AMESim environment [30].

For this purpose, we first created a model of the battery prototype in AMESim software. This model took in to account the module geometry, the mass and the thermal characteristics of different components (cell, resin matrix, aluminium shell with embedded heat sinks) and finally the heat generated from cells. It is assumed that the temperature was homogeneous within each cell. A 28 elements mesh was generated for 2D modelling of the resin matrix. Each cell was surrounded by two resin matrix nodes: a and b (Fig. 9). The aluminium shell was modelled using 14 elements corresponding to the 14 exterior resin matrix nodes b. The two smaller walls of the module were considered adiabatic and an overall heat transfer coefficient h_{wall} was employed in order to model the cooling effect of the heat sinks at the two larger walls.

Hence, the cell energy balance could be expressed as below:

$$m_{cell}Cp_{cell}\frac{dT_{cell}}{dt} = \phi - q_{cell\to a} - q_{cell\to b} \quad (2)$$

The energy balances for resin matrix nodes a and b are the following:

$$m_{a}Cp_{resin}\frac{dT_{a}}{dt} = q_{cell\to a} - \sum_{i} q_{a\to a^{i}} - q_{a\to b} \quad (3)$$

Table 2
Schematic of various fan area obstruction levels.

Ratio of the obstructed fan inlet area	Illustration
0%	
50%	

$$m_{b}Cp_{resin}\frac{dT_{b}}{dt} = q_{cell\to b} - q_{b\to a} - \sum_{i} q_{b\to b^{i}} - q_{b\to wall} \quad (4)$$

Finally, the energy balance for the wall is:

$$m_{wall}Cp_{wall}\frac{dT_{wall}}{dt} = q_{b\to wall} - \sum_{i} q_{wall\to wall^{i}} - h_{wall}A(T_{wall} - T_{amb}) \quad (5)$$

where: $q_{cell\to a}$ and $q_{cell\to b}$ are the heat transfer rates from each cell to its surrounding resin matrix nodes a and b respectively,

$q_{a\to a}$, $q_{a\to b}$, $q_{b\to a}$ and $q_{b\to b}$ are the heat transfer rate between resin matrix nodes,
$q_{b\to wall}$ is the heat transfer rate from exterior resin matrix nodes b to the module wall,
$q_{wall\to wall}$ is the heat transfer rate between module wall nodes.

This AMESim model was validated using data from experiments with the battery prototype under adiabatic and forced convection conditions. Under adiabatic condition, the overall heat transfer coefficient was considered equal to zero. In cases of forced convection, the overall heat transfer coefficient after stabilization can be determined as below:

$$h_{wall} = \frac{14\phi}{A(T_{wall} - T_{amb})} \quad (6)$$

Fig. 10 compares the temperature profiles obtained with simulation to those measured during tests. For all tests, the simulation results corresponded well to the experimental data; consequently, the AMESim model of the battery prototype could be validated. The validation of the AMESim model under adiabatic test condition showed that the used heat calculation method gave an accurate estimation of the battery global heat under charge sustaining mode.

In order to estimate cell temperature at different locations of the battery cooled with heat pipe modules, the aforementioned AMESim model of the battery prototype was slightly modified. Since the copper plate played the role of the battery module wall, all

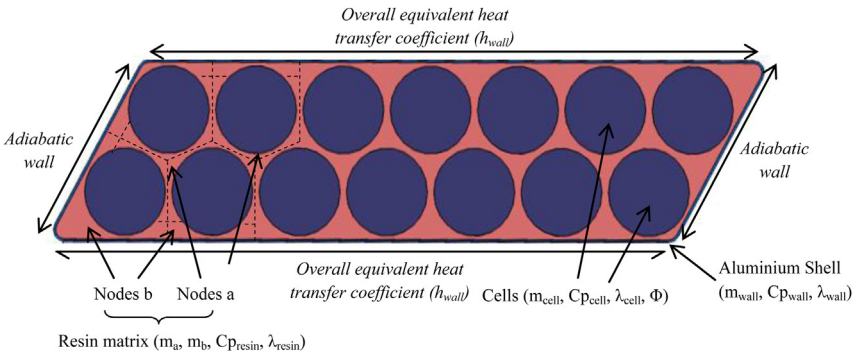

Fig. 9. Battery module scheme and data used for AMESim modelling.

elements corresponding to the aluminium shell with embedded heat sinks of the battery prototype were removed from the model. An overall equivalent heat transfer coefficient was introduced to model the cooling effect of the experimented heat pipes cooling systems. This overall equivalent heat transfer coefficient could be determined using the heater/cooling system interface temperatures measured after stabilization.

$$h_{equi} = \frac{P}{A(T_{evaporator} - T_{amb})} \tag{7}$$

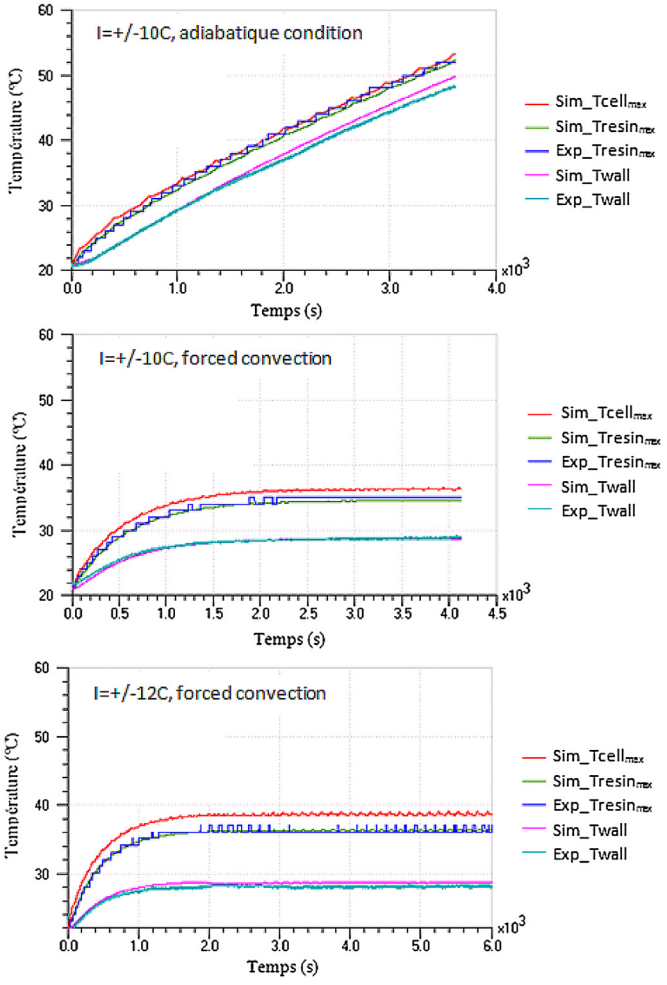

Fig. 10. Battery module scheme and data used for AMESim modelling.

The thermal resistance of the heat pipes cooling systems could be calculated using the following formula:

$$R = \frac{1}{h_{equi}A} \tag{8}$$

The cell temperature at different locations of the module could be evaluated using this modified AMESim model.

3.2. Tests in various positions

We first performed experiment in vertical position under an input power of 38 W. After stabilization (6000 s), the fin temperature ($T_{condenser}$) was around 46.5 °C for both the cooling modules and the heater/copper plate interface temperature ($T_{evaporator}$) reached 51 °C (Fig. 11a). As the evaporator temperature corresponding to that of the battery module wall exceeded 50 °C, it was obvious that natural convection was not sufficient to keep cells in the module within it desired temperature range. However, to evaluate the influence of the inclination, the experiment was pursued under natural convection condition and the experimental apparatus was inclined with an angle of +20° and −20° form the vertical position.

In a heat pipe, the liquid was pumped from the condenser section to the evaporator section thanks to the capillary force. However, the liquid return could be assisted or opposed by the gravity, according to the heat pipe's position. Fig. 11b shows a very slender evolution of the heater/heat pipe interface temperature when the heat pipe cooling modules are used in inclined positions. This means that the capillary effect plays a major role in the liquid transport and the gravity is relatively insignificant. Consequently, the experimented heat pipe cooling system works efficiently under different grade road conditions.

The heat pipe modules were also tested in horizontal position, under natural convection. The thermal performance in horizontal position was found to be far less effective than that in vertical and inclined positions. Table 3 shows a temperature difference of 10 °C between horizontal and vertical positions.

Since the gravity force was found to be negligible in the liquid return mechanism, we believe that the thermal performance degradation in horizontal position is due to a better heat transfer between the fin block and the surround air in vertical or slight inclined positions. Fig. 12 explains the air movement in natural convection for cooling systems in vertical and horizontal position. It is well known that due its lower density, the hot air rises up vertically. When heat pipe modules are in vertical position, the air's vertical movement makes it flows between the fins of the condenser section. Heat exchange with the ambient is enhanced consequently. In horizontal position, the air does not flow through

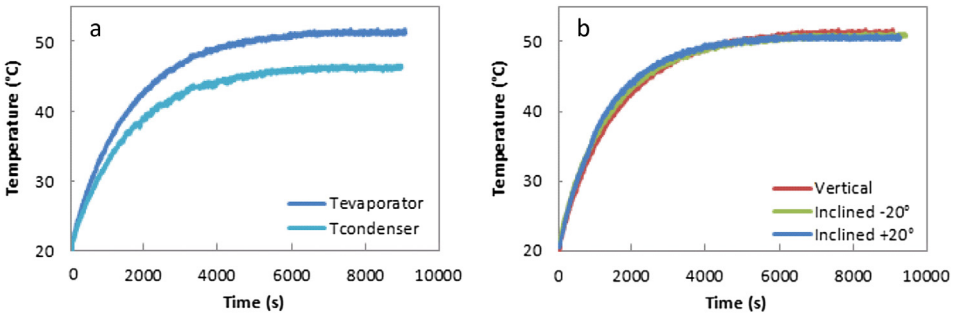

Fig. 11. (a) Vertical position: temperature profile under 38 W input power and natural convection. (b) Influence of inclination.

Table 3
Thermal performance of the system in vertical and horizontal positions.

Input power	38 W	
Heat pipe	Vertical	Horizontal
$T_{evaporator}$ (°C)	51	61
$T_{condenser}$ (°C)	46.5	56

the fins leading to a poor heat evacuation at the condenser block and thus, a higher temperature at the evaporator section.

In order to validate the use of heat pipe in automotive application, aside from the impact of the inclination due different grade roads, investigation on the influence of the vehicle shock and vibration to the heat pipe thermal performance is unavoidable. In our study, the heat pipe cooling system was not tested under vibration environment; however, the influence of vibration on the heat transfer of microgroove has been investigated recently by Guo et al. [31]. It has been found that the vibration movement enlarge the wetting area and intensified consequently the heat transfer of the microgroove. Consequently, the heat pipe seems to be able to work under vibration environment without any thermal performance degradation.

3.3. Chimney cooling

In order to enhance heat exchange at the condenser section, heat pipe cooling modules was coupled with a chimney ventilation structure. Experiments were performed under three input power levels. We attempted to measure the air velocity at the outlet of the chimney. However, the anemometer did not detect any air flow with velocity within the range of 0.15–30 m s^{-1}. We believe that the air velocity though the fins is increased with the chimney structure but was still lower than 0.15 m s^{-1}.

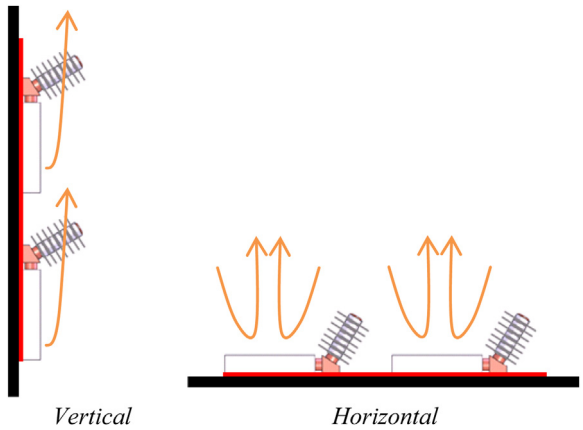

Fig. 12. Schematic of the air movement for cooling system in vertical and horizontal position.

Table 4 presents the evaporator temperature for heat pipe cooling in natural convection and for heat pipe cooling coupled with chimney structure. Associating the heat pipe modules with chimney structure showed noticeable reduction of the temperature compare with natural convection. However, the evaporator temperature still exceeded 50 °C for both 54 W and 84 W input powers. When the heat generated by cell was moderate (38 W), the evaporator temperature was keep at 46 °C. However, using the AMESim model presented previously, the cells temperature was found to be equal to 49.70 °C, which is very close to the upper limit of the battery operating temperature range. Consequently, the chimney structure was not sufficient to keep cell within the desired temperature range.

3.4. Influence of the air forced cooling configuration

Two forced convection configurations could be used to increase heat exchange at the condenser section. Their thermal performance was evaluated under 54 W input power condition. The fan PWM was first set at its minimal value (15% PWM). The air velocity at the outlet of the upper fin block was 1.5 m s^{-1} and 1.2 m s^{-1} for the first and the second configuration respectively. The difference of the air velocity between two configurations at iso fan PWM could be explained on one hand by the pressure drop along the confined section of the second configuration, especially when air flowed through the first fin block. On the other hand, this air velocity deviation could also be due to the accuracy of the anemometer (±3% of reading + 0.05 m s^{-1} for air flow ranging from 0.15 to 3 m s^{-1} and ±3% of reading +0.2 m s^{-1} for air flow ranging from 3.1 to 30 m s^{-1}). However, the evaporator temperature measured for both configurations at 15% PWM was similar. We believed the lower thermal performance due to lower air velocity at the upper fin block of the second configuration was counterbalanced by the larger heat exchange area of this configuration. Indeed, in the first configuration, due to air flows orientation, heat was mainly dissipated through the fin blocks whereas in the second configuration, heat was also evacuated though the two aluminium blocks surface.

Table 4
Copper plate/heater interface temperature for heat pipe coupled with chimney ventilation.

Input power	38 W	54 W	84 W
Free convection	51 °C	58 °C	71 °C
Chimney effect	46 °C	53 °C	66 °C

Table 5
Comparison of the thermal performance between two air ventilation configurations.

Fan fontal area		100%	50%
1st	V_{air}	1.5 m/s	0.5 m/s
	$T_{evaporator}$	29 °C	32 °C
configuration	$T_{cell\ max}$	34.15 °C	37.18 °C
2nd	V_{air}	1.2 m/s	0.5 m/s
	$T_{evaporator}$	28.5 °C	31 °C
configuration	$T_{cell\ max}$	33.64 °C	36.17 °C

To reduce the air velocity, the fan aspiration area was obstructed of 50%. The air velocity was this time similar for both configurations. Lower air velocity may have reduced the pressure drop along the second configuration. The thermal performances were very similar between two configurations. Compared with the case where the fans were not obstructed, the thermal performance degradation was slight whereas the air velocity decreased drastically.

Overall, the thermal performances of two configurations were similar when fans were used under iso conditions (PWM rate and obstructed area ratio) (see Table 5). However, the second configuration only employed three fans instead of six for the first one. Consequently, the parasitic power consumption and the global air flow were two times lower for the second configuration. Moreover, using fewer fans also helped reduce the noise level of vehicles. Finally, in the second configuration, heat pipes worked in an enclosed space, which meant the heat pipe cooling system could be easily implemented in vehicles. For the above reasons, the second configuration was judged to be more adequate.

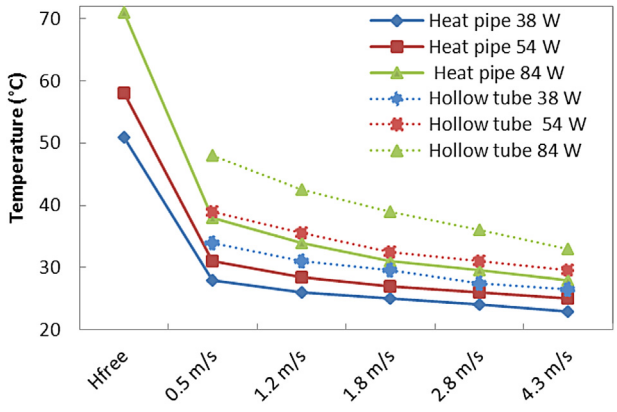

Fig. 13. Thermal performance of the heat pipe cooling coupled with the second ventilation configuration.

3.5. Thermal performance panel of the second configuration

The thermal performance of the heat pipes associated with the second ventilation configuration was evaluated under three input power levels: 38 W, 54 W, 84 W. For each input power, the fans were set at different PWM levels from 15% PWM to 25%, 50% and 95% PWM, giving an air velocity of 1.2 m s^{-1}, 1.8 m s^{-1}, 2.8 m s^{-1} and 4.3 m s^{-1} respectively. At lowest fan PWM, the fan aspiration area was obstructed of 50% in order to get low air velocity of 0.5 m s^{-1}. The evaporator temperature, corresponding to the wall temperature of the module, is presented in Fig. 13.

For comparison purpose, we also performed tests with cooling modules made of hollow tubes. Theoretically, due to the lack of working fluid, the heat amount transferred to the fin block was lower for the hollow tube, leading to a lower temperature at this section. Heat input was not evacuated efficiently causing a higher temperature at the evaporator section. The results for hollow tube shown in dotted lines in Fig. 13 were coherent with the above theory. Under high power input and low ventilation rate, hollow pipes cooling degraded the temperature up to 10 °C compare with heat pipes cooling.

The temperature distribution at different locations of the module was determined using the AMESim model. The hottest cells were the two cells in the centre and the coolest cells were those in the four corners of the module. However, the temperature gradient was found to be lower than 1.5 °C for all tests. The thermal resistance and the highest cell temperature of each configuration were reported in Table 6. We noticed that for the lowest battery heat generation rates, the cells were over-cooled even under restricted air flows (15% PWM with fan area obstructed or not). This means the air flow could be reduced even more. At high battery heat generation rates, the cells could be maintained within its optimal temperature range using very low ventilation rates (15% PWM with fan area obstructed or not). Increasing the air velocity appeared to be useless. At the highest heat generation rate, cells temperatures did not exceed 50 °C if fans were set at the lowest PWM level (15%). However, a moderate ventilation rate (25% PWM) was required to keep the cells temperatures within the optimal range. When the air velocity was increased greatly (more than two times higher), the cells temperatures dropped very slightly. This thermal behaviour was similar to that observed for the two lower heat generation rates. Consequently, combining heat pipes cooling modules with low velocity cooling at the condenser section appeared to be the best compromise between the energy consumption, the noise level and the thermal performance.

3.6. Further discussion

In real life driving conditions, battery power solicitation profiles are always dynamic. Consequently, heat profiles generated from

Table 6
Thermal performance of heat pipe cooling system coupled with the second ventilation configuration.

Input power			38 W		54 W		84 W	
Fan PWM	Fan section	V_{air} (m/s)	R (°C/W)	T_{cell_max} (°C)	R (°C/W)	T_{cell_max} (°C)	R (°C/W)	T_{cell_max} (°C)
15% (min)	50%	0.5	0.184	31.64	0.185	36.17	0.202	46.05
15% (min)	100%	1.2	0.132	29.62	0.139	33.64	0.155	41.91
25%	100%	1.8	0.105	28.61	0.111	32.13	0.119	38.99
50%	100%	2.8	0.079	27.60	0.093	31.12	0.101	37.47
95% (max)	100%	4.3	0.053	26.60	0.074	30.12	0.083	35.97

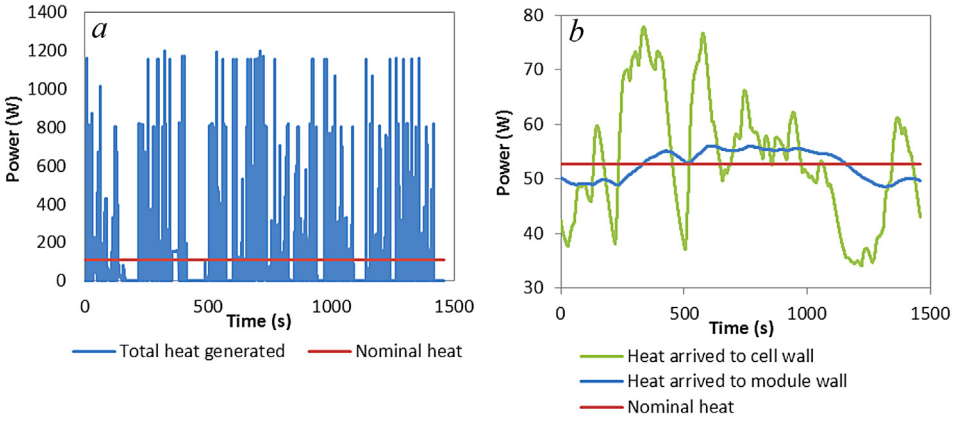

Fig. 14. (a) Heat profile generated from cells in the module. (b) Heat profile at module wall and at cell wall.

batteries are of large amplitude and high frequency, unlike those produced by other electronic and electric devices. Fig. 14a presents variable heat rejected by cells in the battery module during standard driving cycle. The nominal value of the heat generated was found to be slightly over 100 W, which corresponds to the second power level experimented in this work. We can clearly see that the transient heat generated by cells has highly variable amplitudes and short durations.

For battery module with cells inserted in a resin matrix and cooling systems applied to module walls such as in this study case, transient heat arrived to cooling devices was computed using the AMESim model and presented in Fig. 14b. We remarked that the heat profile at cooling wall has slight fluctuation and very smooth shape. This is due to large heat capacity of the cells and the resin matrix. Consequently, the influence of the variation of heat flux on the heat pipe behaviour would be very slim in this study case. To evaluate the cell temperature fluctuation under transient heat input, simulations were made by repeating several times the heat profile in Fig. 14a. Fig. 15 shows that after stabilization, the cell temperature fluctuation during each cycle was about 4 °C, which is still lower than the critical value (5 °C). We also remarked that the temperature range found for cell under variable heat generated condition corresponded to that obtained preciously for cell under 108 W constant power input.

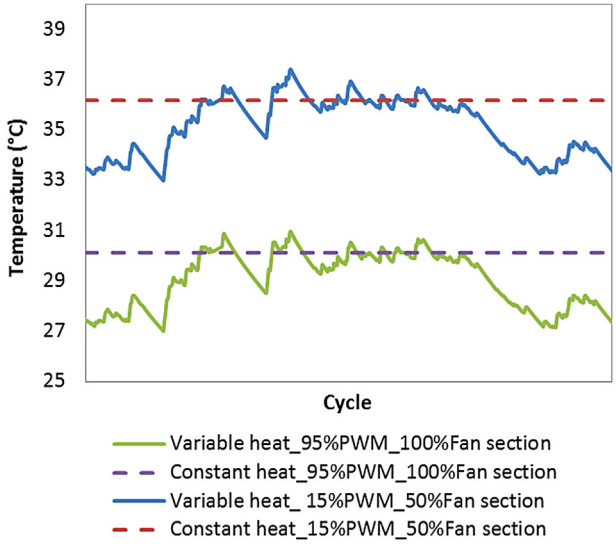

Fig. 15. Cell temperature under transient heat input and different cooling conditions.

Finally, in case of larger variation in cell heat loss or lower module heat capacity or direct contact between cooling device and cells, heat arrived to cooling system may vary rapidly and have larger amplitude; hence, the transient behaviour of the heat pipe would be more prominent and investigation of this transient behaviour is necessary. In future work, we will investigate the transient behaviour of the heat pipe for configuration where cooling device is in direct contact with cells.

4. Conclusions

In order to extend the battery life and decrease HEV/EV cost, battery should be operated within its optimum temperature range. The use of a heat pipe cooling system for a HEV application lithium-ion battery was considered. According to experimental results, the following conclusions could be drawn:

(1) The experimented heat pipe modules were designed to be used in vertical position; however, it works satisfactorily under different grade road conditions.
(2) Natural convection is not sufficient to keep the battery within its operating temperature range. For better heat evacuation, the condenser section of the heat pipe system needs to be coupled with a ventilation system.
(3) The association of the heat pipe cooling with chimney ventilation was found to improve significantly the heat evacuation without any power consumption. However, its thermal performance is not adequate to keep the cells temperature lower than 50 °C, especially when the battery operates under high load conditions.
(4) Coupled with adequate ventilation configuration, heat pipe is revealed to be a promising cooling solution for HEV/EV battery. Indeed, for all performed battery heat generation rates, cells temperature was maintained within the optimal range under low ventilation rates. Increasing the air velocity does not practically increase the thermal performance. This minimizes power consumption and noise level in the vehicle.
(5) The experiments showed that heat pipe cooling system can work efficiently in enclosed space, which facilitate its implementation in the vehicle.

References

[1] S.S. Zhang, K. Xu, T.R. Jow, J. Power Sources 115 (2003) 137.
[2] J. Fan, J. Power Sources 117 (2003) 170.
[3] Q. Wang, P. Ping, X. Zhao, G. Chu, J. Sun, C. Chen, J. Power Sources 208 (2012) 210.

[4] M. Broussely, S. Herreyre, P. Biensan, P. Kasztejna, K. Nechev, R.J. Staniewicz, J. Power Sources 97-98 (2001) 130.
[5] M.S. Wu, P.C.J. Chiang, Electrochim. Acta 52 (2007) 3719.
[6] P. Ramadass, B. Haran, R. White, B.N. Popov, J. Power Sources 112 (2002) 614.
[7] J. Shim, R. Kostecki, T. Richardson, X. Song, K.A. Striebeln, J. Power Sources 112 (2002) 222.
[8] G. Sarre, P. Blanchard, M. Broussely, J. Power Sources 127 (2004) 65.
[9] M. Fleckensteina, O. Bohlena, M.A. Roscherb, B. Bäkerc, J. Power Sources 196 (2011) 4769.
[10] Y. Troxler, B. Wu, M. Marinescu, V. Yufit, Y. Patel, A.J. Marquis, N.P. Brandon, G.J. Offer, J. Power Sources (2013).
[11] A.A. Pesaran, J. Power Sources 110 (2002) 377.
[12] C.W. Park, A.K. Jaura, SAE Tech. Pap. (2003).
[13] A.A. Pesaran, Advanced Automotive Battery Conference, 2001.
[14] A.A. Pesaran, in: Fourth Vehicle Thermal Management Systems Conference and Exhibition London, 1999.
[15] H. Park, J. Power Sources 239 (2013) 30.
[16] R. Kizilel, R. Sabbaha, J.R. Selmana, S. AlHallaj, J. Power Sources 194 (2009) 1105.
[17] R. Sabbah, R. Kizilel, J.R. Selman, S. Al-Hallaj, J. Power Sources 182 (2008) 630.
[18] G.H. Kim, J. Gonder, J. Lustbader, A. Pesaran, World Electr. Veh. J. 2 (2008) 46.
[19] Y.T. Chen, S.W. Kang, Y.H. Hung, C.H. Huang, K.C. Chien, Appl. Therm. Eng. 51 (2013) 864.
[20] M. Ameli, B. Agnewa, P.S. Leung, B. Ng, C.J. Sutcliffe, J. Singh, R. McGlen, Appl. Therm. Eng. 52 (2013) 498.
[21] E.T. Mahefkey, M.M. Kreitman, J. Electrochem. Soc. 118 (1971) 1383.
[22] G. Zhang, Z. Wu, Z. Rao, L. Fu, Chem. Ind. Eng. Prog. 28 (2009) 1165 (in Chinese).
[23] M.S. Wu, K.H. Liu, Y.Y. Wang, C.C. Wan, J. Power Sources 109 (2002) 160.
[24] Z. Rao, S. Wang, M. Wu, Z. Lin, F. Li, Energy Convers. Manag. 65 (2013) 92.
[25] D. Bernardi, E. Pawlikowski, J. Newman, J. Electrochem. Soc. 132 (1985) 5–12.
[26] L. Rao, J. Newman, J. Electrochem. Soc. 144 (1997) 2697.
[27] Y. Saito, K. Kanari, K. Takano, J. Power Sources 68 (1997) 451.
[28] K.E. Thomas, J. Newman, J. Power Sources 844 (2003) 119–121.
[29] T.H. Tran, S. Harmand, B. Desmet, F. Pailhoux, J. Electrochem. Soc. 160 (2013) 775–780.
[30] http://www.lmsintl.com/LMS-Imagine-Lab-AMESim.
[31] C. Guo, X. Hu, W. Cao, D. Xu, D. Tang, Appl. Therm. Eng. 52 (2013) 385.